Radiation Physics and Chemistry xxx (xxxx) xxx–xxx

Contents lists available at ScienceDirect

Radiation Physics and Chemistry

journal homepage: www.elsevier.com/locate/radphyschem

Investigation of the effect of titanium dioxide and clay grafted with glycidyl methacrylate by gamma radiation on the properties of EVA flexible films

Suellen Signer Bartolomei[a,b], Julyana Galvão Santana[a], Francisco R. Valenzuela Díaz[b], Pınar Akkas Kavaklı[c], Olgun Guven[c], Esperidiana A.B. Moura[a,*]

[a] Center for Chemical and Environmental Technology, Nuclear and Energy Research Institute, CQMA/IPEN-CNEN/SP, Sao Paulo, Brazil
[b] Metallurgical and Materials Engineering Department, Polytechnic School, University of Sao Paulo, Sao Paulo, SP, Brazil
[c] Hacettepe University, Department of Chemistry, Polymer Chemistry Division, Beytepe, Ankara, Turkey

ARTICLE INFO

Keywords:
Nanofillers
Dispersion
Graft polymerization
Functionalization of nanofillers

ABSTRACT

Many studies report that nanocomposites obtained by dispersion of a small amount nanofiller into the polymer have remarkable improvements achieved in the mechanical and physical properties. However, in order to achieve this great improvement in properties, it is necessary that the nanofillers be dispersed homogeneously into the polymeric matrix. Often this dispersion is difficult to achieve due to the high interfacial energy of the nanoparticles present. This study reports the effect of gamma irradiation induced graft of glycidyl methacrylate (GMA) onto the surface of TiO2 and Clay nanofillers to improve their dispersion into the EVA matrix. The physical and mechanical properties of Ethylene-vinyl acetate copolymer (EVA) flexible films with these nanoparticles were studied. EVA nanocomposite with adding of the different amount of TiO2 and modified montmorillonite clay grafted and un-grafted with glycidyl methacrylate (GMA) using gamma irradiation have been prepared by melt extrusion. The nanocomposite flexible films were produced using a flat die extrusion process. The PGMA-grafted nanofillers were characterized by XRD and TEM analysis. The flexible films were characterized by Tensile tests, ATR–FTIR, UV–VIS, XRD, TG, and FE-SEM analysis to understand the nature of the interaction between the nanofillers and EVA matrix. The results showed that the addition of PGMA-grafted TiO2 and Clay nanofillers into EVA matrix improved the bonding between the nanofillers and matrix. It was also found that the PGMA-grafted nanofillers could be well dispersed into an EVA matrix in contrast to that of un-grafted. The tensile strength and modulus of the resulting EVA/TiO2-PGMA enhanced in comparison to that of un-grafted TiO2. The EVA/Clay-PGMA had slightly decreased tensile strength comparable to that of EVA/Clay but had considerably improved elastic modulus. In addition, the flexible films based on TiO2 exhibited high UV–Vis light absorption with energy gap shifted to the visible region. The results demonstrated that TiO2 and Clay nanofillers grafted with GMA by gamma radiation can be used to prepare EVA flexible films with improved bonding between the nanofillers and matrix and, consequently, enhanced properties for food and cosmetic packaging application.

1. Introduction

Since the eighties, hybrid organic-inorganic nanocomposites obtained from the dispersion of inorganic solid nanofiller in the polymeric matrix have been intensely investigated due to the remarkable improvements achieved in the properties when a small amount of nanofillers are added to a polymer matrix. The remarkable improve on physical and mechanical properties of polymers due to the addition of inorganic solid nanofiller may be explained because of their high specific surface area that increases the interaction between the nanofiller in different ways and the number of dispersed-matrix interactions, increasing the effects on the global properties of the nanomaterial (Faruk et al., 2012).

Polymer nanocomposites can be prepared by in-situ polymerization, solution mixing or melt intercalation. The melt intercalation process has been reported to have several advantages over the others, such as the relative simplicity of the process, the use of conventional polymer processing equipment, continuous and large-scale production, and consequently, more efficient and economical production from of the industrial viewpoint. However, the dispersion of nanofillers in a polymer matrix by melt intercalation processing still presents great challenges due to the tendency of nanofillers form aggregates into most

* Corresponding author.
E-mail address: eabmoura@ipen.br (E.A.B. Moura).

https://doi.org/10.1016/j.radphyschem.2018.08.022
Received 27 April 2018; Accepted 21 August 2018

of the polymer matrices. In addition, the incompatibility between hydrophilic nanofillers and hydrophobic polymers also may lead to poor interfacial adhesion, bad dispersion of nanofillers in a matrix and the production of the material with unsatisfactory properties.

There are many papers on the great importance of nanofiller-matrix interface adhesion in the preparation of polymer nanocomposites by melt intercalation process. Many studies have shown that the poor interfacial adhesion between the nanofiller and matrix may decrease the nanocomposite performance yielding a material with low properties. On the other hand, a well-dispersed system added to good interface adhesion between nanofillers and a matrix will lead to the production of nanomaterials with more desirable properties (Goffin, et al., 2011; Kango et al., 2013).

In order to homogenize the dispersion of the nanofillers in the polymeric matrix during the mechanical processing in the molten state, several strategies have been employed. Among them, It must be emphasized that the addition of compatibilizing agents during the processing, the surface treatment and chemical functionalization of nanofillers as a measure to increase hydrophobicity and interfacial adhesion through physical interaction or chemical bonding between the matrix and the dispersed phase (Rong et al., 2006; Thakur et al., 2013).

The functionalization of nanofillers can be accomplished by means of the grafting polymerization of polymeric macromolecules with functional groups on their surface, obtaining a material with new properties, but still with the original physical characteristics. The grafting polymerization of macromolecules in nanoparticles can be induced by high energy radiation (gamma radiation, electron beam) or chemically initiated, grafting by the chemical method, however, these technics differ in many respects. Radiation grafting has many advantages over other conventional methods because it does not require the use of the catalysts or additives to initiate the reaction. Thus, unlike the chemical initiation method, the radiation-induced process is free of contamination, leaves no chemical residues, so that the purity of the processed products can be maintained. In most cases of grafting initiated by high energy radiation, the reactions are not temperature dependent, the processes are homogeneous and easy to control (Barsbay and Güven, 2009; Barsbay et al., 2014; Kavaklı, et al., 2007; Rymuszka et al., 2017; Wu et al., 2005; Zhang et al., 2001).

Titanium dioxide (TiO_2) is widely used in various food, medical and biological products (Vejdan et al., 2016; Kaewklin et al., 2018). The incorporation of TiO_2 nanoparticles into polymeric matrix is being studied extensively because of their remarkable properties. The TiO_2 is a non-toxic, free from pollution, high oxidation power, a chemically inert material, UV light stability, and exhibit antimicrobial activity (He et al., 2016; Vejdan et al., 2016). TiO2 presents ethylene photo-degradation activity when exposed to UV light by generating of hydroxyl radicals and another reactive oxygen species on its surface, which can reacts with organic molecules (Hussain et al., 2011; Karthikeyan et al., 2017; Kaewklin et al., 2018). These nanoparticles may have their surface modified by several methods; however, it is still difficult to obtain a homogenous and fine dispersion of these nanoparticles into a polymeric matrix nanocomposite (Bhattacharya, 2016; Kango et al., 2013; Li et. al, 2017; Zhao et al., 2012).

Polymeric nanocomposites and organophilic clay, as dispersed phase, have better perform than polymer alone, due to the potentially high-aspect ratio and surface area that could lead to processing of the nanocomposite materials with great property enhancements. Among the properties that are improved, it can be stressed to include the mechanical resistance (increased strength and higher modulus), thermal stability, barrier properties, decreased flammability, resistance to degradation by moisture absorption, besides the reduction of costs and weight. A polymer nanocomposite containing clay must be obtained with layers of clays exfoliated, a process not easily achieved due to the intrinsic incompatibility of hydrophilic clays and hydrophobicity of most of the engineering polymers. Generally, a surface treatment with quaternary ammonium salts is performed and exfoliates the clay particles by expanding the basal spacing. For a polymer containing polar functional groups, an alkylammonium surfactant is a suitable filler that promotes formation of the nanocomposite under optimum processing conditions. However, to improve the dispersion of nanoclay in polymers by mechanical processing in the molten state, other forms of modification must be studied, such as grafting polymerization of PGMA induced by gamma radiation (Bhattacharya, 2016; Campos et al., 2017; Kango et al., 2013; Mahmoodian et al., 2010; Tsotetsi et. al., 2017).

This work presents the effects of the incorporation of titanium dioxide and clay nanofillers grafted with GMA by gamma radiation on properties of EVA flexible films.

Table 1
Formulation of the nanocomposite flexible films.

Materials	EVA/clay (%, wt.)	EVA/clay grafted (%, wt.)	EVA/TiO_2 (%, wt.)	EVA/TiO_2 grafted (%, wt.)
EVA	99.5 – 98.5	99.5 – 98.5	99.5 – 98.5	99.5 – 98.5
Clay	0.5; 1.0; 1.5	–	–	–
Clay-PGMA	–	0.5; 1.0; 1.5	–	–
TiO_2	–	–	0.5; 1.0; 1.5	–
TiO_2-PGMA	–	–	–	0.5; 1.0; 1.5

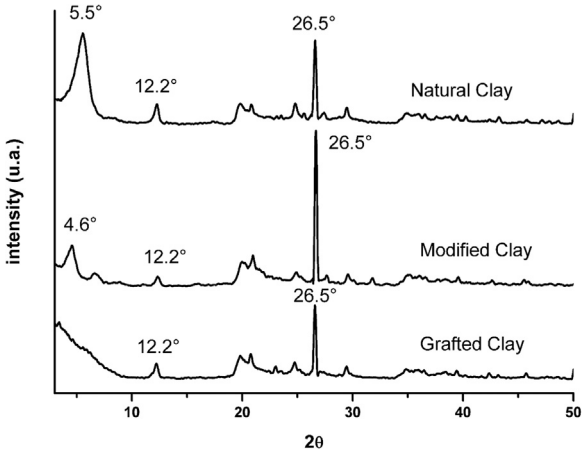

Fig. 1. XRD patterns of natural, modified with quaternary ammonium salt and grafted with GMA Clay.

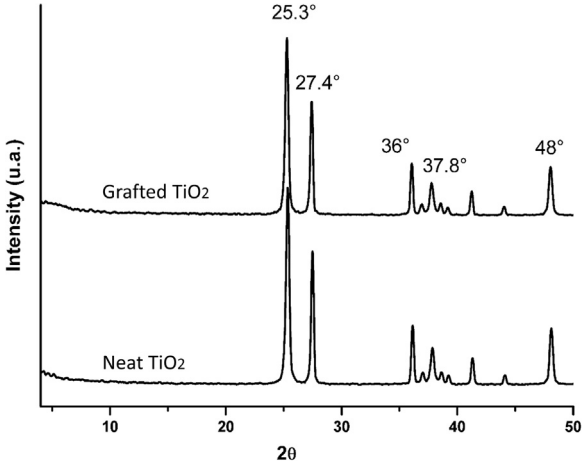

Fig. 2. XRD patterns of neat and grafted with PGMA TiO_2.

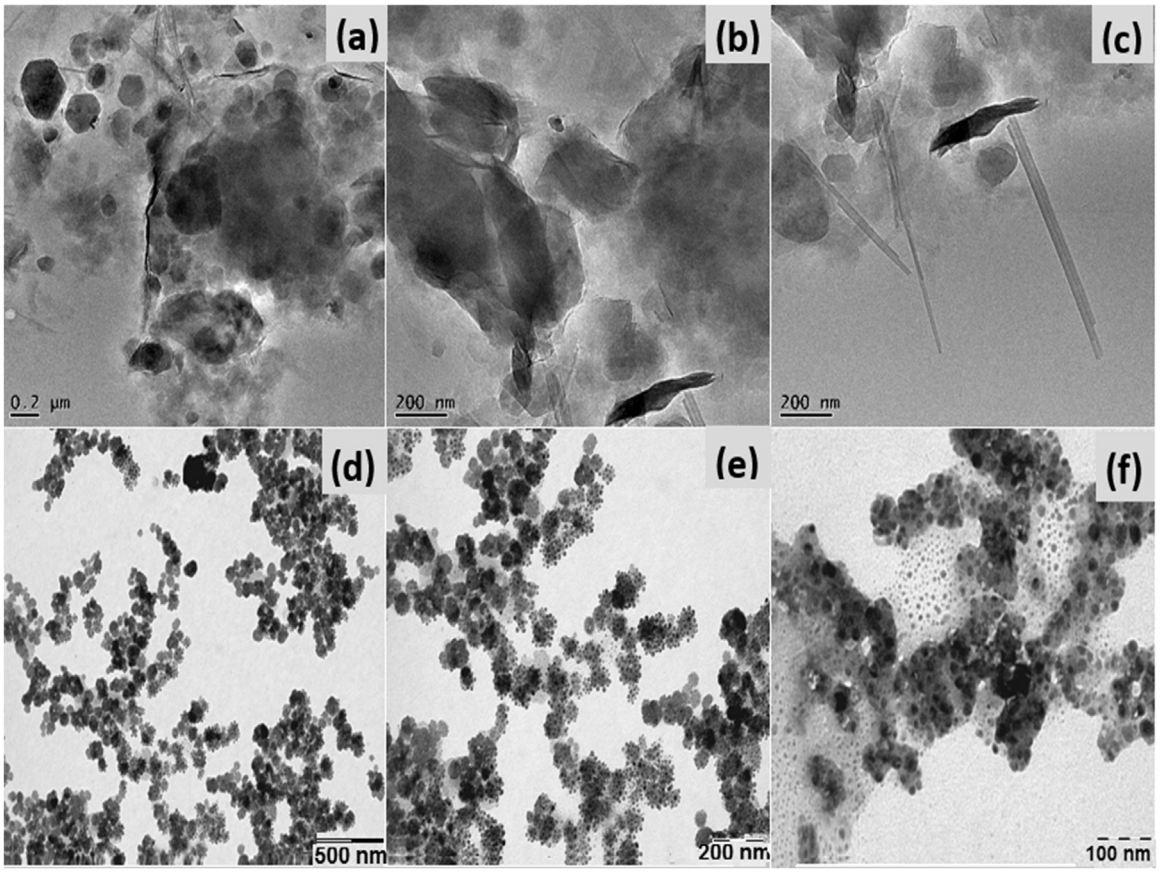

Fig. 3. TEM images of modified Clay in Fig. (a) = 0.2 µm, 3(b) = 200 nm and 3(c) = 100 nm size; and Clay grafted with GMA in (d) = 500 nm, 3(e) = 200 nm and 3(f) = 100 nm size, respectively.

2. Experimental

2.1. Materials

Ethylene vinyl acetate copolymer (EVA), MFI = 20.14 g/10 min at 190 °C, 2.16 kg, with 28 mol% of vinyl acetate, from Braskem. Natural Light Green Clay. Titanium dioxide (TiO_2) with particle size of 30 nm supplied by Degussa AG (Dusseldorf, Germany). Analytical grade glycidyl methacrylate (GMA, 97%, Aldrich). The solvents dimethyl formamide (DMF) and ethanol were purchased from Casa Americana.

2.2. Clay preparation

Natural light green clay was firstly modified with sodium carbonate (Na_2CO_3). In this process, calcium (Ca^{2+}) counter ions were exchanged by sodium (Na^+). Secondly, quaternary ammonium salt was added into the resulting product and mixed. Finally, the dispersed organophilized clay mixture was filtered, washed with deionized water and dried at 60 °C.

2.3. Grafting procedure

A solution of 300 mL with 70% DMF and 30% ethanol together with 5% wt. of nanofillers was prepared and submitted to a mechanical mixer for 1 h. GMA was dissolved in the initial solution to prepare monomer solutions with 7% wt. and then the mixture was deoxygenated by bubbling with high purity N_2 gas for 20 min. The deoxygenated mixtures were irradiated with gamma rays from a ^{60}Co source (absorbed dose 10 kGy, dose rate of 6 kGy/h) at room temperature. After irradiation, in order to remove the remaining GMA monomer, the samples were washed 3 times with DMF, centrifuged at 3900 rpms for 5 min, then, washed 4 times with methanol and centrifuged at 3900 rpms for 5 min. The samples were then dried in an air-circulating oven at 45 °C for 24 h, disaggregated and characterized. This procedure was repeated to preparer clay and TiO_2 grafted with poly(glycidyl methacrylate) (PGMA).

2.4. EVA nanocomposites and flexible films preparation

All EVA nanocomposites with adding of different amount of TiO_2 and modified natural light green clay grafted and un-grafted PGMA, respectively, as presented in Table 1, were prepared by melt extrusion using a twin-screw extruder HAAKE Rheomex P332, 16 mm and L/D = 25 rate from Thermo Scientific. The temperature profile used during processing was 100/110/125/130/135/140 °C and the screws rotation were 50 rpms. The extrudates coming out of the extruder were cooled down for a better dimensional stability, pelletized by a pelletizer. The nanocomposite materials were fed into a flat die single extruder for flexible films preparation. The temperature profile used during the films preparation in single screw extruder was 100/110/125/130/135/140 °C and the screws rotation were 80 rpms.

2.5. Characterization

2.5.1. Tensile tests

Tensile specimens were obtained in the way of process and in longitudinal way from the films samples in order to evaluate the mechanical behavior. The tests were carried out using an INSTRON Universal Testing Machine, model 5564 according to ASTM D 882-91 standard at 25 °C and a loading rate of 10 mm/min, in six test specimens of each prepared nanocomposite and the average values were reported.

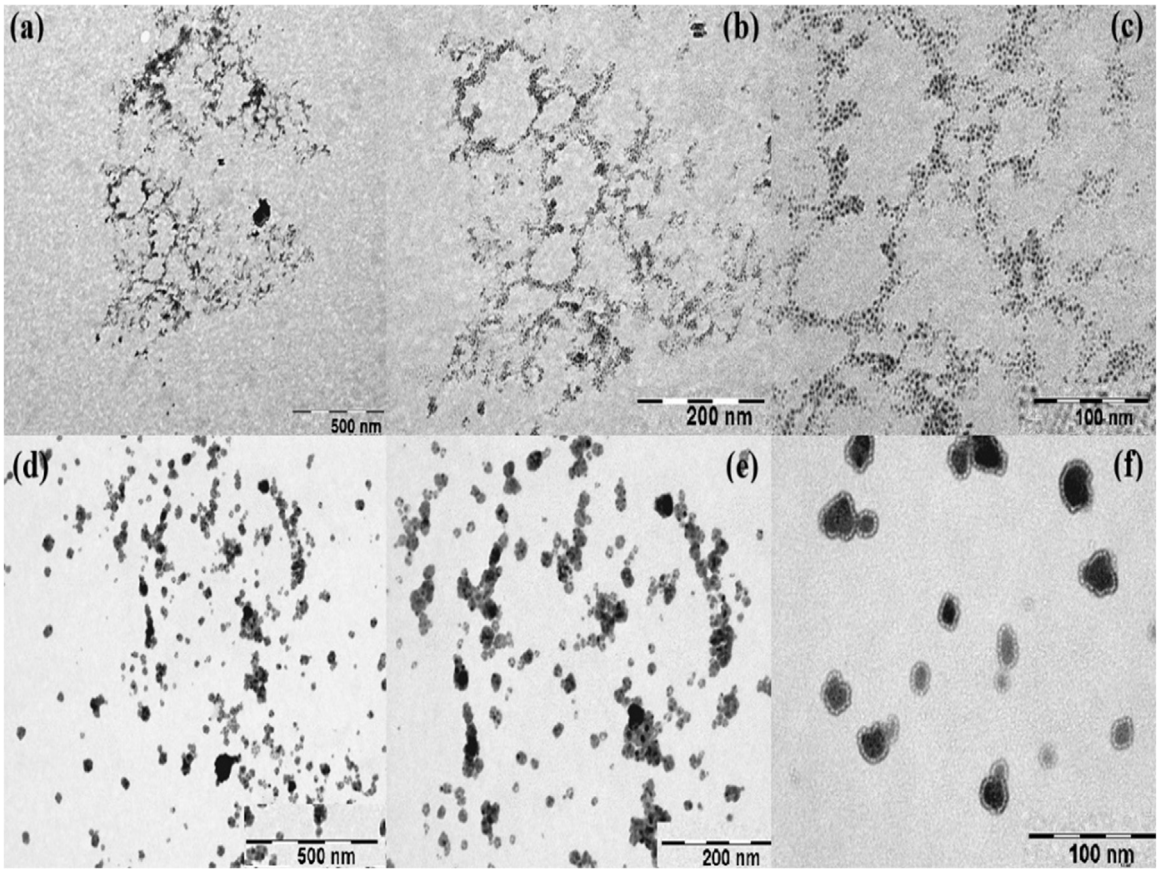

Fig. 4. TEM images of neat TiO_2 in (a) = 500 nm, 4(b) = 200 nm and (c) = 100 nm size respectively; and TiO_2 grafted with GMA in (d) = 500 nm, 4(e) = 200 nm and 4(f) = 100 nm size, respectively.

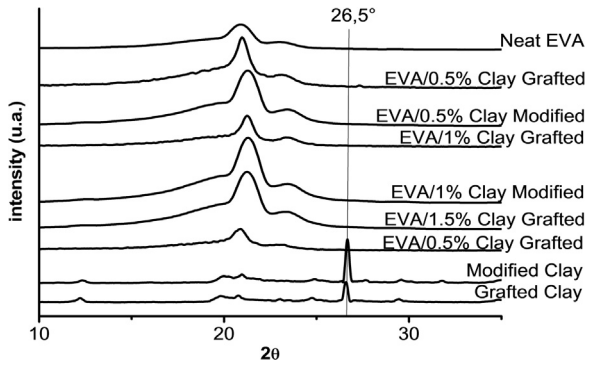

Fig. 5. XRD diffraction patterns for the EVA and its nanocomposites with modified clay and grafted Clay with PGMA.

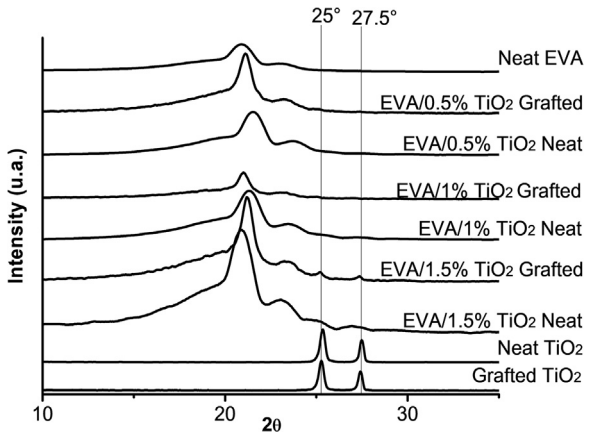

Fig. 6. XRD diffraction patterns for the EVA and its nanocomposites with neat TiO_2 and TiO_2-grafted with PGMA.

2.5.2. X Rays Diffraction (XRD)

In this study was used to evaluate the modification of natural ligth green clay and the intercalation in the EVA matrix. XRD patterns for the samples were recorded on a Philips XPERT-MPD diffractometer with CuKα radiation (λ = 1.54 nm) operated at 40 kV and 40 mA, with 2θ varying between 2° and 50°.

2.5.3. Thermogravimetric analysis (TG)

TG analysis were carried out using TGA/SDTA851e (Mettler Toledo). The samples were heated from 30° to 600°C under a nitrogen atmosphere (50 mL/min) at heating rate of 20 °C/minute.

2.5.4. UV–vis absorption spectroscopy

UV–vis of nanocomposite sheets was conducted with a Cary 1E spectrophotometer with the wavelength ranging from 200 to 800 nm.

2.5.5. ATR- FTIR

The FTIR spectra of the samples were obtained with a UATR two, Perkin Elmer spectrometer. Spectra were recorded accumulating 64 scans at 4 cm^{-1} resolution in Attenuated Total Reflection (ATR) mode using a single reflection diamond crystal.

2.5.6. Field emission scanning electron microscopy (FE-SEM)

The samples' cryofractured morphology were studied using a Quanta FEG 650 scanning electron microscope at 15 kV. The specimens were fractured in liquid nitrogen.

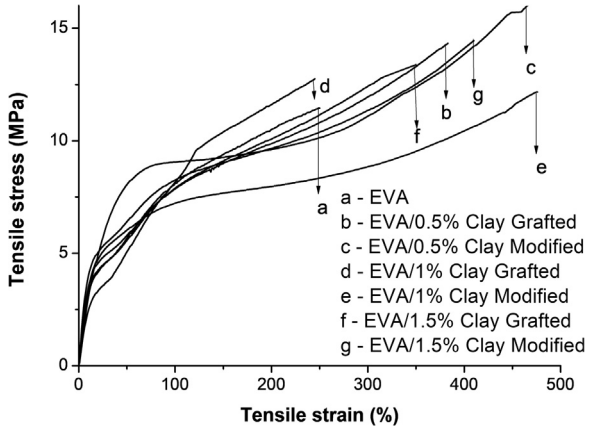

Fig. 7. Tensile stress–strain curves for neat EVA, EVA/Clay and EVA/grafted Clay with PGMA flexible films.

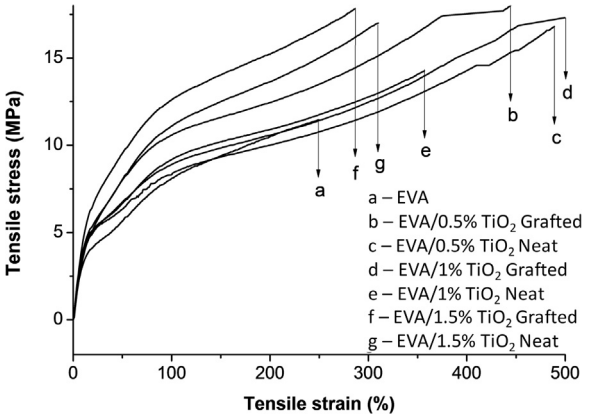

Fig. 8. Tensile stress–strain curves for neat EVA and its nanocomposites with TiO_2 and grafted TiO_2 with PGMA flexible films.

2.5.7. Transmission electron microscopy (TEM)

Clay and TiO2 nanofillers and two nanocomposites were observed using a Jeol-1010 with 80 kV electron acceleration voltage and increases until 60.000 times.

3. Results and discussion

3.1. Nanofillers results

3.1.1. XRD analysis results of Clay

3.1.1.1. XRD patterns of natural, modified and grafted Clay are showed in Fig. 1. The XRD patterns of natural light green clay presented in Fig. 1 show three peaks with major intensity, one at $2\theta = 5.5^{\circ}$ (d001) corresponding to an interlayer distance of 1.6 nm, this peak corresponding to the basal spacing montmorillonite. A second peak at $2\theta = 12.2^{\circ}$ corresponding to kaolinite and the last one at $2\theta = 26.5^{\circ}$ corresponding to quartzo. After modification of clay, the XRD patterns presented a small shift to the left from $2\theta = 5.5^{\circ}$ to $2\theta = 4.6^{\circ}$ corresponding to an increase interlayer distance to 1.92 nm. This increase confirms the intercalation of the quaternary ammonium cation in the interlamellar spacings of clay. In XRD analysis results of grafted clay show no characteristic montmorillonite peak at the range of $2\theta = 4.6^{\circ}$, suggesting that PGMA chains has diffused into the gallery of the clay and that the clay has been exfoliated (Banerjee et al., 2013; Suter et al., 2015).

3.1.1.2. XRD patterns of neat and grafted TiO_2 are showed in Fig. 2. As shown in the Fig. 2, XRD patterns presented peaks around 2θ of 25.3° (101), 37.8° (004), 48° (200), which could be indexed to the characteristic peaks of anatase TiO_2, and also the peaks 27.4° (110) and 36° (101) characteristic of rutile TiO_2. After grafting procedure of TiO_2 the XRD patterns did not show shift significant (Li et al., 2018, 2017).

3.1.2. Transmission electron microscopy (TEM) results

3.1.2.1. TEM analysis results of modified and grafted Clay. TEM micrographs analysis results of modified and grafted Clay are showed in Fig. 3. The images of modified Clay with 0.2 μm, 200 nm and 100 nm size are presented in Fig. (a), (b) and (c) respectively. The images of Fig. (d), (e) and (f) correspond to Clay grafted with GMA at size of 500 nm, 200 nm and 100 nm, respectively. In Fig. (a), (b) and (c), it can be seen that the modified clay presents nanosheets with some agglomerated. The Fig. (d), (e) and (f) shows the GMA polymerized on the surface of the clay nanosheets which caused better dispersion of the nanoparticles.

3.1.2.2. TEM analysis results of neat TiO_2 and grafted TiO_2. Fig. 4 shows the TEM micrographs analysis results of neat TiO_2 and grafted TiO_2. The images of neat TiO_2 with 500 nm, 200 nm and 100 nm size are presented in Fig. 4(a), Figs. 4(b) and 4(c); and TiO_2 grafted with GMA in Figs. 4(d), 4(e) and 4(f), respectively. Comparing these images, it can be seen that the size of the grafted particles appears to be larger than non-grafted particles, this is due to the polymerization of GMA on the surface of titanium dioxide. Spherical and homogeneous structures with a ring due to PGMA grafted on the surface of TiO_2 can be seen in the in Fig. (f). On the other hand, no spherical structures can be clearly seen in the TEM image of neat TiO2, Fig. (a-b), indicating that nanoparticles, in this case, are adhering to one another.

3.2. Nanocomposites characterization results

3.2.1. XRD analysis results of nanocomposites

3.2.1.1. XRD patterns of neat EVA and EVA/Clay nanocomposites. Fig. 5 shows the XRD patterns of neat EVA and EVA/Clay nanocomposites. As can be seen in this Fig. the XRD pattern of neat EVA shown two peaks around 21 and 23°, corresponding to (110) and (200), respectively, which present a strong amorphous halo. Regarding the addition of modified and grafted clay into EVA matrix the Fig. 5 shows no characteristic clay peaks in XRD pattern of EVA/Clay modified and EVA/Clay grafted. These results suggest a homogeneous dispersion of the clay nanosheets in the polymeric matrix.

Table 2
tensile tests results of neat EVA, EVA/Clay and EVA/Clay/PGMA flexible films.

Samples	Tensile strength at break (MPa)	Elongation at break (%)	Young's modulus (GPa)
Neat EVA	14.16 ± 1.2	238.73 ± 6.86	3.25
EVA/Clay/PGMA 0.5%	14.95 ± 0.5	251.00 ± 3.45	3.71
EVA/Clay 0.5%	16.43 ± 1.2	290.51 ± 3.93	3.52
EVA/Clay/PGMA 1.0%	13.04 ± 0.9	168.72 ± 5.7	4.81
EVA/Clay 1.0%	12.41 ± 1.0	301.81 ± 7.37	2.57
EVA/Clay/PGMA 1.5%	13.38 ± 0.93	218.03 ± 7.34	3.89
EVA/Clay 1.5%	14.45 ± 0.67	260.03 ± 7.12	3.51

Table 3
tensile tests results of flexible films: EVA/TiO_2 and EVA/TiO_2 grafted with PGMA.

Samples	Tensile strength at break (MPa)	Elongation at break (%)	Young's modulus (GPa)
Neat EVA	14.16 ± 1.2	238.73 ± 6.86	3.25
EVA/ TiO_2/PGMA 0.5%	18.59 ± 1.16	250.48 ± 8.59	4.42
EVA/ TiO_2 0.5%	16.81 ± 0.9	293.60 ± 8.19	3.57
EVA/ TiO_2/PGMA 1.0%	17.51 ± 1.0	284.97 ± 8.12	3.83
EVA/ TiO_2 1.0%	14.25 ± 1.0	205.64 ± 4.18	3.10
EVA/ TiO_2/PGMA 1.5%	18.02 ± 1.6	245.51 ± 8.57	4.04
EVA/ TiO_2 1.5%	14.40 ± 1.2	277.99 ± 8.35	3.65

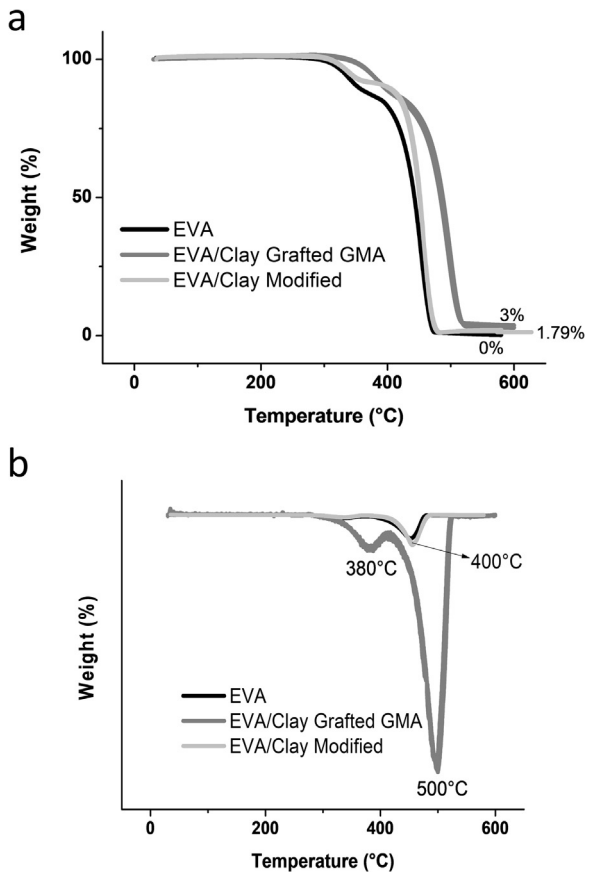

Fig. 9. TG thermograms (9a) and DTG (9b) of neat EVA and its nanocomposites with clay.

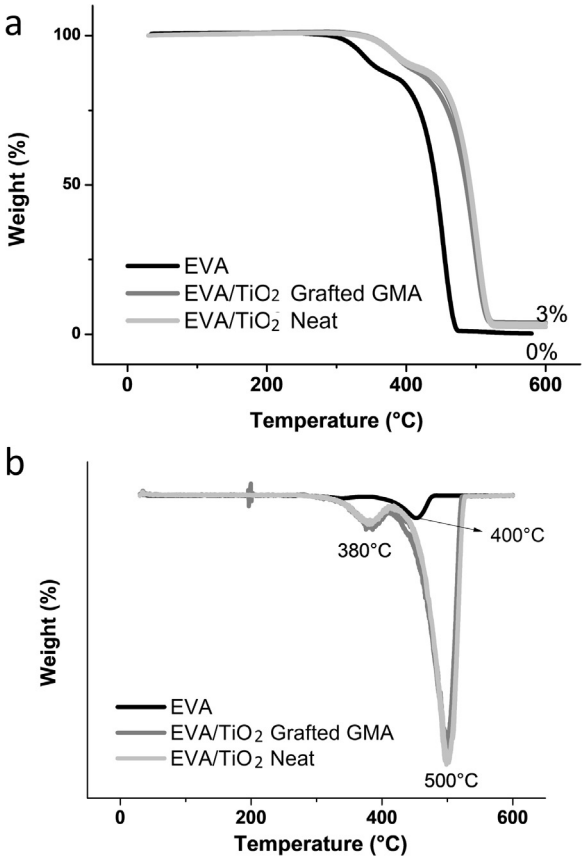

Fig. 10. TG thermograms (8a) and DTG (8b) of neat EVA and its nanocomposites with TiO_2.

3.2.1.2. XRD patterns of neat EVA and EVA/TiO_2 nanocomposites. In Fig. 6, it can be observed that the two prominent 2θ peaks at around 25° and 27.5° of TiO_2 disappeared after the addition of 0.5% and 1% in EVA matrix. For the EVA with 1.5% of TiO_2 addition, it is noticed that the intensity of the peaks was reduced but they are still present, indicating that there are some agglomerates of TiO_2 Grafted in the EVA matrix.

3.2.2. Mechanical tests results

3.2.2.1. Mechanical tests results of neat EVA and EVA/Clay nanocomposites. The mechanical tests results of neat EVA and EVA/Clay nanocomposites are showed in Fig. 7 and Table 2. The results presented shows the average values calculated from the data obtained in tests of five test specimens.

From of the Fig. 7, it can be seen the tensile stress–strain curves for neat EVA and its nanocomposites with modified Clay and grafted Clay with PGMA. This figure shows that tensile strength and Young's modulus of neat EVA increases significantly with the increase of Clay addition.

The Table 2 presents the tensile tests results for neat EVA, EVA/Clay and EVA/grafted Clay with PGMA flexible films.

From Table 2 it can be seen:

- a slight increase of the tensile strength at break for EVA/Clay in comparison with EVA/Clay/GMA;
- the values of Young's modulus are significantly higher when the grafted Clay with PGMA are incorporated into EVA matrix;
- for 1.0% wt. Clay, grafted with GMA added the Young's modulus increased around 90% in comparison with EVA/Clay flexible film. Whereas that the Young's modulus is a measure of the stiffness of a material, how much it can resist plastic deformation, and the higher the value of Young's modulus of one material, stiffer is the material when subjected to tensile deformation. Then, these results show that the incorporation of Clay grafted with GMA increases the stiffness of EVA/Clay films. Osman et al. (2017) prepared EVA (18% wt. of vinyl acetate) with 5% of organically modified montmorillonite clay pre-dispersing in toluene and deionized water solution, homogenized by using ultrasonication method. They verified a decrease in Young's modulus of the nanocomposites accompanied by the increase in elongation at break and toughness.

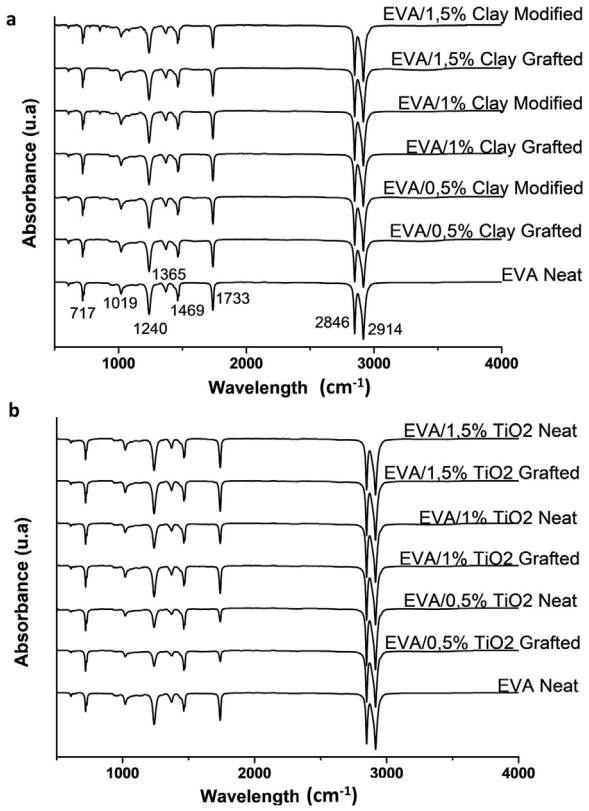

Fig. 11. FTIR spectra for the neat EVA, the EVA/Clay (9a) and for the EVA/TiO_2 (9b) nanocomposites in the range 4000–400 cm^{-1}.

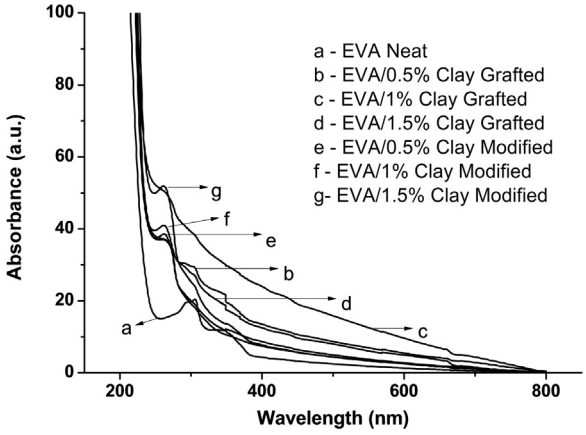

Fig. 12. UV–vis spectra for the neat EVA and for the EVA/Clay.

3.2.2.2. Mechanical tests results of neat EVA and EVA/Clay nanocomposites. The mechanical tests results of neat EVA and EVA/TiO_2 nanocomposites are showed in Fig. 8 and Table 3. The results presented shows the average values calculated from the data obtained in tests for five test specimens.

Fig. 6 show the tensile stress–strain curves for neat EVA and its nanocomposites with TiO_2 and grafted TiO_2 with PGMA flexible films. From this figure, it can be seen that tensile strength and Young's modulus of neat EVA increases significantly with the addition of grafted TiO_2-PGMA into EVA matrix.

Table 3 presents the results of tensile tests of neat EVA, EVA/TiO_2 and EVA/TiO_2 grafted with PGMA flexible films.

From Table 3 it can be seen:

- high increase of the tensile strength at break for EVA/TiO_2/GMA in comparison with EVA/TiO_2 without GMA;
- high increase of Young's modulus of the EVA/TiO_2/GMA in comparison with EVA/TiO_2 without GMA.

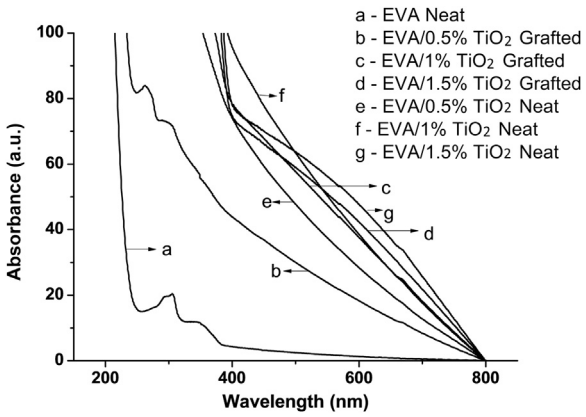

Fig. 13. UV–vis spectra for the neat EVA and for the EVA/TiO_2.

Table 4
Absorbance values at 500 nm in Uv–vis spectra to EVA and its nanocomposites.

Samples	Abs (a.u.)	Samples	Abs (a.u.)
Neat EVA	2.4	Neat EVA	2.4
EVA/Clay/PGMA 0.5%	8.6	EVA/ TiO_2/PGMA 0.5%	30
EVA/Clay 0.5%	5	EVA/ TiO_2 0.5%	48
EVA/Clay/PGMA 1.0%	16	EVA/ TiO_2/PGMA 1.0%	58
EVA/Clay 1.0%	4.4	EVA/ TiO_2 1.0%	63
EVA/Clay/PGMA 1.5%	8	EVA/ TiO_2/PGMA 1.5%	60
EVA/Clay 1.5%	4.4	EVA/ TiO_2 1.5%	64

The increases in tensile strength and elastic modulus of the film are probably due to the high crystallinity of TiO_2, as is evidenced by the crystalline peaks around 2θ of 25.3°, characteristic of anatase TiO_2, and 2θ of 27.4°, characteristic of rutile TiO_2 in the XRD pattern. Based on this, it is possible to infer that the incorporation of TiO_2 into EVA matrix strengthens the network structure of the EVA film, improved, consequently its tensile strength and elastic modulus. These results are in accordance with those of Kaewklin, *et. al.* (2018) and He et al. (2016). Kaewklin, et al. added 1% in wt. TiO_2 nanopowders in the chitosan matrix and they observed a significant increase of around 60% in tensile strength of chitosan/TiO_2 film and a decrease in elongation at break (Kaewklin, et. al, 2018).

3.2.3. Thermogravimetric analysis (TG) results

Fig. 9 shows the TG (Fig. 9a) and DTG (Fig. 9b) thermograms of EVA and EVA/Clay nanocomposites. The same can be observed in Fig. 10 (TG (Fig. 10a) and DTG (Fig. 10b)) for the EVA/TiO_2 nanocomposites. As expected, EVA showed two-step degradation which can be related to deacetylation and main-chain decomposition at around 380 and 400 °C respectively.

TG of the nanocomposites with Clay e TiO_2 showed a great difference in weight loss and in the onset temperature when compared with the neat EVA. Furthermore, there was an increase in the final degradation temperature of the nanocomposites with Clay and TiO_2, from 400° to 500°C, this phenomenon shows an improvement in the thermal stability of the nanocomposites.

3.2.4. FTIR analysis results

Fig. 11 shows the FTIR spectra of neat EVA samples and their nanocomposites. All the absorption peaks assigned to EVA are in agreement with others reports. The peak at 1733 cm^{-1} is from C=O vibration, at 1240 cm^{-1} and 1019 cm^{-1} is from C-O stretching, these three due to the polar VA groups. The other spectrum is due to ethylene groups in

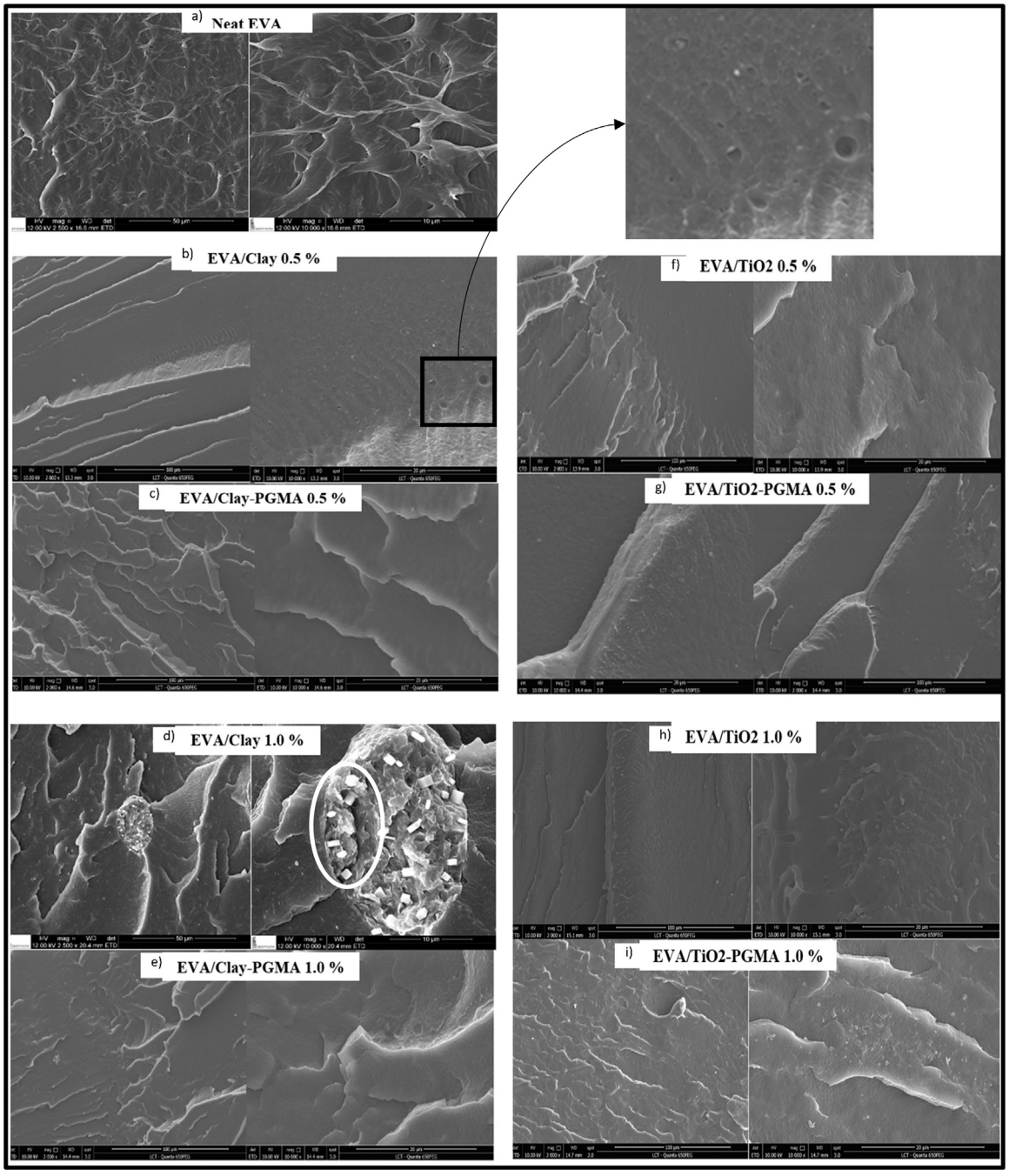

Fig. 14. FE-SEM images of neat EVA (a) and its nanocomposites with modified Clay (b, d); grafted Clay with PGMA (c, e); neat TiO_2 (f, h) and grafted TiO_2 (g, i).

EVA as the peaks at 2914 cm^{-1} and 2856 cm^{-1} related to C-H asymmetric and symmetric vibration, the peak at 1469 cm^{-1} is due to C-H bending deformation. The peak at 1365 cm^{-1} is from -CH_3 symmetric deformation, and the peak at 717 cm^{-1} is assigned to C-H rocking deformation. (Campos et al., 2017; Wang et al., 2013; Zhao et al., 2012) The addition of nanofillers and PGMA did not caused significant changes in positions or intensities of peaks in FTIR spectrum.

3.2.5. UV–vis analysis results

Upon visual examination, EVA/Clay nanocomposites samples presented a slight yellowish coloration and EVA/TiO_2 nanocomposites samples presented whitish coloration. The intensity of such alterations increased with nanofillers percentages. Fig. 12 (EVA/Clay) and 13 (EVA/TiO_2) show the changes in absorption UV–vis spectra of EVA and its nanocomposites films with equal thickness Fig. 13).

Table 4 shows a comparison of the absorbance values by reference to the wavelength of 500 nm. The absorbance values for the nanocomposite with TiO_2 were higher than the values of the nanocomposite with Clay. However, PGMA grafting in the clay improved significantly the UV barrier. The best UV barrier with clay was achieved using 1% Clay grafted with PGMA (16%), considering the nanocomposites with TiO_2, as might be expected, the UV barrier improved significantly for all addition of TiO_2.

3.2.6. Field Emission Scanning Electron Microscopy (FE-SEM) analysis results

FE-SEM micrographs of cryofractured surfaces of the neat EVA and its nanocomposite specimens were studied to understand the failure mechanisms and also study the interaction between different components. FE-SEM micrographs of neat EVA and its nanocomposite in

different magnifications are showed in Fig. 14. Fig. (14a) is an overview of neat EVA. Micrographs surface of EVA nanocomposite with 2.000X and 10.000X of magnifications are showed in Fig. (14 b-i). These images showing a better and uniform dispersion for the grafted nanofillers with PGMA incorporated into EVA matrix when compared with a non-homogeneous distribution of un-grafted nanofillers.

According to micrograph surface samples of Fig. 14, it is possible to notice a large difference between the fractured region of the neat EVA and its composites. The micrograph surface of neat EVA shows high deformation, characteristic of a ductile fracture. However, the micrograph surface of nanocomposites presents a flat surface with low deformation that suggests a brittle failure processes.

The highlighted areas of Figs. 14b and 14(d), EVA/Clay 0.5% and EVA/Clay 1% respectively, show several agglomerates, cracks, cavities and voids between clay and matrix that result in poor adhesion between clay and matrix strength. These regions of defects were not observed after GMA grafting procedure of clay, that also improving the dispersion of the clay nanosheets into the EVA matrix, as showed in Figs. 14c and 14(e).

It can be seen in Figs. 14f and 14(h), there are regions with large numbers of agglomerates into the nanocomposites EVA/TiO_2 0.5% and EVA/TiO_2 1%, once again the grafting was efficient, resulting in a reduction of the agglomerates into the EVA matrix with 0.5% and 1% Grafted TiO_2, Figs. 14g and14i, respectively.

4. Conclusion

This work presented an investigation on the effect of titanium dioxide and clay grafted with glycidyl methacrylate by gamma radiation on the properties of EVA flexible films. The results showed that the addition of TiO_2 and Clay surface grafted with GMA into EVA matrix improved the bonding between the nanofillers and matrix. It was also found that the PGMA-grafted nanofillers could be well dispersed into EVA matrix in contrast to that of un-grafted.

The tensile strength and modulus of the resulting EVA/TiO_2-PGMA enhanced in comparison to that of un-grafted TiO_2. The EVA/Clay-PGMA had slightly decreased tensile strength comparable to that of EVA/Clay but had considerably improved elastic modulus. In addition, the flexible films based on TiO_2 and Clay grafted exhibited high UV–Vis light absorption with energy gap shifted to the visible region. In conclusion, the results demonstrated that TiO_2 and Clay nanofillers grafted with GMA by gamma radiation can be used to prepare EVA flexible films with improved bonding between the nanofillers and matrix and, consequently, enhanced properties for food and cosmetic packaging application.

Acknowledgements

The authors wish to thank Coordenação de Aperfeiçoamento de Pessoal de Nível Superior - CAPES, Brazil, and Conselho Nacional de Desenvolvimento Científico e Tecnológico - CNPq, Brazil to provide the support for this work.

References

Tsotetsi, T.Abel, Jonas Mochane, M., Elias Motaung, T., Patricia Gumede, T., Linda Linganiso, Z., 2017. Synergistic effect of EG and cloisite 15A on the thermo-mechanical properties and thermal conductivity of EVA/PCL blend. Mater. Res. 20 (1), 109–118. https://doi.org/10.1590/1980-5373-MR-2016-0277.

Banerjee, S., Joshi, M., Ghosh, A.K., 2013. Investigations on Clay dispersion in polypropylene/clay nanocomposites using rheological and microscopic analysis. J. Appl. Polym. Sci. 4464–4473. https://doi.org/10.1002/APP.39590.

Barsbay, M., Güven, O., 2009. A short review of radiation induced raft-mediated graft copolymerization: a powerful combination for modifying the surface properties of polymers in a controlled manner. Radiat. Phys. Chem. 78, 1054–1059.

Barsbay, M., Kodama, Y., Güven, O., 2014. Functionalization of cellulose with epoxy groups via initiated RAFT-mediated grafting of glycidyl methacrylate. Cellulose 21, 4067–4079.

Bhattacharya, M., 2016. Polymer nanocomposites-A comparison between carbon nanotubes, graphene, and clay as nanofillers. Materials 9 (4), 1–35. https://doi.org/10.3390/ma9040262.

Campos, L.M.P., Zaharescu, T., Boaro, L.C., Santos, L.K.G., Santos, T.M.R., Ferreira, H.P., Parra, D.F., 2017. Thermal and mechanical behavior evaluation of dental composites filled with irradiated montmorillonite. J. Appl. Polym. Sci. 134 (29), 45063.

Faruk, O., Andrzej, K., Bledzki, H-P., Fink, M.S., 2012. Biocomposites reinforced with natural fibers: 2000–2010. Progress. Polym. Sic. 37 (11), 1552–1596.

Goffin, A.L., Raquez, J.M., Duquesne, E., Habibi, Y., Dufresne, A., Dubois, P., 2011. Poly (ε-caprolactone) based nanocomposites reinforced by surface-grafted cellulose nanowhiskers via extrusion processing: morphology, rheology, and thermo-mechanical properties. Polymer **52** (7), 1532–1538.

He, Q., Zhang, Y., Cai, X., Wang, S., 2016. Fabrication of gelatin–TiO_2 nanocomposite film and its structural, antibacterial and physical properties. Int. J. Biol. Macromol. 84, 153–160.

Hussain, M., Bensaid, S., Geobaldo, F., Saracco, G., Russo, N., 2011. Photocatalytic degradation of ethylene emitted by fruits with TiO_2 nanoparticles. Ind. Eng. Chem. Res. 50, 2536–2543.

Kaewklin, P., Siripatrawan, U., Suwanagul, A., Lee, Y.S., 2018. Active packaging from chitosan-titanium dioxide nanocomposite film for prolonging storage life of tomato fruit. Int. J. Biol. Macromol. 112, 523–529.

Kango, S., Kalia, S., Celli, A., Njuguna, J., Habibi, Y., Kumar, R., 2013. Surface modification of inorganic nanoparticles for development of organic-inorganic nanocomposites - a review. Progress. Polym. Sci. 38 (8), 1232–1261. https://doi.org/10.1016/j.progpolymsci.2013.02.003.

Karthikeyan, K.T., Nithya, A., Jothivenkatachalam, K., 2017. Photocatalytic and antimicrobial activities of chitosan-TiO_2 nanocomposite. Int. J. Biol. Macromol. 104, 1762–1773.

Kavaklı, P.A., Seko, N., Tamada, M., Güven, O., 2007. Radiation-induced graft polymerization of glycidyl methacrylate onto pe/pp nonwoven fabric and its modification toward enhanced amidoximation. J. Appl. Polym. Sci. 105, 1551–1558.

Li, H., Dong, W., Xi, J., Du, G., Ji, Z., 2018. 3D flower like TiO_2/GO and TiO_2/MoS_2 heterostructures with enhanced photoelectrochemical water splitting. J. Mater. Sci. 53, 7609–7620. https://doi.org/10.1007/s10853-018-2051-8.

Li, Y.S., Qin, J.T., Han, Y., Du, J.F., Dong, Z.B., Sun, S.F., Liu, Y., 2017. Controlled preparation and highly photocatalytic activity of portable MCC-g-GMA@TiO2 photocatalyst by pre-radiation grafting-embedding method. Appl. Catal. B: Environ. 218, 101–110. https://doi.org/10.1016/j.apcatb.2017.03.083.

Mahmoodian, M., Pourabbas, B., Amirhosein Baghaee Arya, 2010. Preparation and characterization of Bis-GMA/TEGDMA/Clay nanocomposites at low filler content regimes. J. Compos. Mater. 44 (11), 1379–1395. https://doi.org/10.1177/0021998309353675.

Osman, A.F., Fitri, T.F.M., Rakibuddinb, M., Hashimc, F., Johari, Syed, A.T.T., Ananthakrishnan, R., Ramli, R., 2017. Pre-dispersed organo-montmorillonite (organo-MMT) nanofiller: morphology, cytocompatibility and impact on flexibility, toughness and biostability of biomedical ethyl vinyl acetate (EVA) copolymer. Mater. Sci. Eng. C 74, 194–206.

Rong, M.Z., Zhang, M.Q., Ruan, W.H., 2006. Surface modification of nanoscale fillers for improving properties of polymer. Mater. Sci. Technol. 22, 787–796.

Rymuszka, D., Terpiłowski, K., Sternik, D., Tomczynska-Mleko, M., Goncharuk, O., 2017. Wettability and thermal analysis of hydrophobic poly(methyl methacrylate)/silica nanocomposites. Adsorpt. Sci. Technol. 35 (5–6), 560–571.

Suter, J.L., Groen, D., Coveney, P.V., 2015. Mechanism of exfoliation and prediction of materials properties of clay − polymer nanocomposites from multiscale modeling. Nano Lett. 15, 8108–8113.

Thakur, V.K., Thakur, M.K., Gupta, R.K., 2013. Graft copolymers from cellulose: synthesis, characterization and evaluation. Carbohydr. Polym. 14, 18–25.

Vejdan, A., Ojagh, S.M., Adeli, A., Abdollahi, M., 2016. Effect of TiO2 nanoparticles on the physico-mechanical and ultraviolet light barrier properties of fish gelatin/agar bilayer film. LWT Food Sci. Technol. 71, 88–95.

Wang, X., Cooney, R.P., Ray, S., Kilmartin, P.A., Jin, J., 2013. The effect of matrix polarity on the properties of poly(o-methoxyaniline)–EVA blends. Mater. Chem. Phys. 141 (1), 180–188. https://doi.org/10.1016/j.matchemphys.2013.04.044.

Wu, C.L., Zhang, M.Q., Rong, M.Z., Friedrich, K., 2005. Silica nanoparticles filled polypropylene: effects of particle surface treatment, matrix ductility and particle species on mechanical performance of the composites. Compos Sci. Technol. 65, 635–645.

Zhang, M.Q., Rong, M.Z., Zeng, H.M., Schmitt, S., Wetzel, B., Friedrich, K., 2001. An atomic force microscopy study on structure and properties of irradiation grafted silica particles in polypropylene based nanocomposites. J. Appl. Polym. Sci. 80, 2218–2227.

Zhao, X., Zhang, W., Chen, S., Zhang, J., Wang, X., 2012. Hydrophilicity and crystallization behavior of PVDF/PMMA/TiO2(SiO2) composites prepared by in situ polymerization. J. Polym. Res. 19 (5). https://doi.org/10.1007/s10965-012-9862-0.